Earth and Planetary Science Letters 593 (2022) 117679

Contents lists available at ScienceDirect

Earth and Planetary Science Letters

www.elsevier.com/locate/epsl

Highly heterogeneous mantle caused by recycling of oceanic lithosphere from the mantle transition zone

Shengping Qian [a,*], Vincent Salters [b], Alex J. McCoy-West [c], Jonny Wu [d], Estelle F. Rose-Koga [e], Alexander R.L. Nichols [f], Le Zhang [g], Huaiyang Zhou [a,*], Kaj Hoernle [h,i]

[a] State Key Laboratory of Marine Geology, Tongji University, Shanghai, China
[b] Depart. of Earth Ocean and Atmospheric Science and NHMFL, Florida State University, Tallahassee, USA
[c] Isotropics Geochemistry Laboratory, School of Earth and Environmental Science, James Cook University, Townsville, Australia
[d] Depart. of Earth & Atmospheric Sciences, University of Houston, Houston, USA
[e] Université Clermont Auvergne, CNRS, IRD, OPGC, Laboratoire Magmas et Volcans, F-63000 Clermont-Ferrand, France
[f] School of Earth and Environment, University of Canterbury, Private Bag 4800, Christchurch 8140, New Zealand
[g] State Key Laboratory of Isotope Geochemistry, Guangzhou Institute of Geochemistry, Chinese Academy of Sciences, Guangzhou, China
[h] GEOMAR Helmholtz Centre for Ocean Research Kiel, 24148 Kiel, Germany
[i] Kiel University, Institute of Geosciences, 24118 Kiel, Germany

ARTICLE INFO

Article history:
Received 9 December 2021
Received in revised form 27 May 2022
Accepted 8 June 2022
Available online 21 June 2022
Editor: R. Hickey-Vargas

Keywords:
South China Sea
mantle transition zone
recycled oceanic crust
EMII and FOZO
mantle heterogeneity

ABSTRACT

Geochemical heterogeneities observed in the mantle are usually attributed to recycling of oceanic lithosphere through subduction. However, it remains hotly debated where recycled material stagnates, and how quickly it can be liberated back to surface. This knowledge gap hinders our understanding of mantle circulation and the chemical evolution of the Earth. Here we address these questions using a combination of geochronology and geochemistry from South China Sea (SCS) seamounts. The Shixingbei seamount lavas formed during active seafloor spreading at c. 19.1 Ma show limited geochemical variability, whereas the Zhenbei-Huangyan seamount chain formed during the post-spreading stage at c. 7.8 Ma and displays a wide range of compositions. However, melt inclusions in olivine and plagioclase from the Zhenbei-Huangyan basalts show considerably greater isotopic variability than seen in the whole rock compositions of both the SCS syn- and post-spreading lavas. A previously unidentified third mantle source component (FOZO) revealed by olivine-hosted melt inclusions along with both depleted (DMM) and enriched (EMII) mantle components is required in the source region to explain the observed isotopic and chemical variability. On the basis of our results, the age of the recycled ocean crust and sediments in this region are estimated to be c. 120 – 350 Ma. We infer that these enriched components in the SCS lavas come from the mantle transition zone. Variations in mantle source heterogeneity coupled with melting process control spatial–temporal (spreading vs. post-spreading stage) geochemical variations of lavas from the SCS and surrounding areas. Together with the results from published studies, we propose that marginal basins are one of the major locations on Earth where oceanic and/or continental lithosphere is transferred into the upper mantle and transition zone, representing an important source of upper mantle heterogeneity. We provide a simple conceptual model linking plate subduction and upper mantle heterogeneity and the volcanism in the SCS and surrounding areas.

1. Introduction

In general, mid-ocean ridge basalts (MORBs) have relatively uniform and overall depleted compositions, while oceanic island basalts (OIBs) display considerable chemical heterogeneity (e.g., Gale et al., 2013; Hoernle et al., 2011; Hofmann, 1997; Jackson and Hart, 2006; Salters and Stracke, 2004; Stracke et al., 2005). Five endmembers are commonly proposed to explain the isotopic heterogeneity observed in oceanic rocks: depleted MORB-source mantle (DMM), enriched mantle one (EMI) and two (EMII), high time-integrated μ ($^{238}U/^{204}Pb$) mantle (HIMU), and a focal zone (FOZO) component (e.g., Hanan and Graham, 1996; Hickey-Vargas, 1992; Stracke et al., 2005; Workman and Hart, 2005; Zindler and

* Corresponding authors.
E-mail addresses: shengpingqian@tongji.edu.cn (S. Qian), zhouhy@tongji.edu.cn (H. Zhou).

https://doi.org/10.1016/j.epsl.2022.117679
0012-821X/

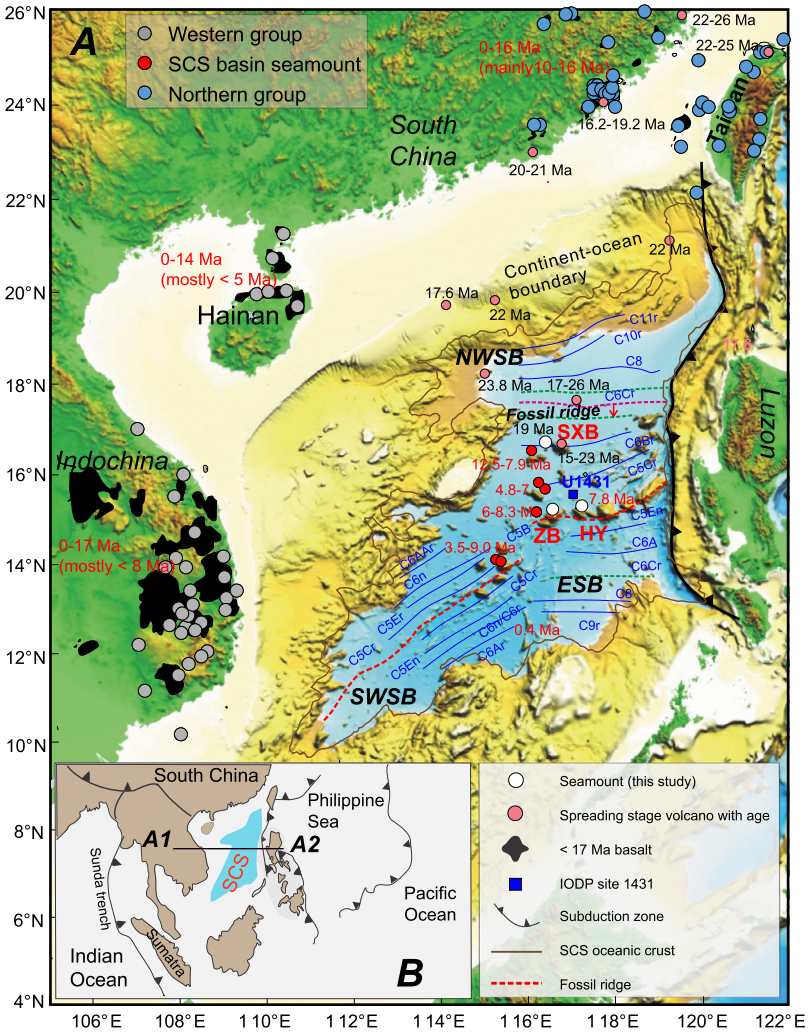

Fig. 1. Simplified geological map of the South China Sea (SCS) and adjacent regions, and sampling locations. (A) Bathymetric map of the present-day SCS and adjacent regions. Distribution of late Cenozoic intraplate volcanism in the SCS basin (red circles) and surrounding area (e.g., western group including Indochina block and Hainan (grey circles); and northern group including Southeast China and Taiwan (blue circles)) are shown with ages labeled in red. Spreading stage volcanism (pink dots) is also shown with ages labeled in black (Age data for both are from the GEOROC database (http://georoc.mpchmainz.gwdg.de/georoc)). Major magnetic anomalies (blue lines) are also shown and marked with anomaly numbers after Li et al. (2014). The red dashed lines show the final fossil ridges and the pink dashed line marks the location of the ridge jump with the arrow indicating the direction of ridge migration. Bathymetric data were taken from GEBCO_2014 Grid (http://www.gebco.net). SXB, Shixingbei; ZB, Zhenbei; HY, Huangyan. ESB, East Sub-basin; SWSB, Southwest Sub-basin; NWSB, Northwest Sub-basin. (B) The major subduction zones surrounding the SCS and the Indochina Peninsula. Inset map showing the location of the tomographic profile (A1-A2) presented in Fig. 9. (For interpretation of the colors in the figure(s), the reader is referred to the web version of this article.)

Hart, 1986). The cause of the geochemical differences between MORBs and OIBs and the chemical heterogeneity of Earth's mantle is mainly attributed to mantle convection, but the understanding of where recycled material stagnates and how it is mingled and arrives back at the surface, is still debated.

MORBs originate from a large-scale homogeneous, incompatible element-poor shallow and degassed mantle, whereas OIBs are related to mantle plumes sampling both ancient undegassed domains and recycled crustal reservoirs (e.g., Castillo et al., 2010; Hofmann, 1997; Jackson and Hart, 2006; McCoy-West et al., 2016; Salters and Stracke, 2004; Stracke et al., 2005; Workman and Hart, 2005; Zindler and Hart, 1986). Nevertheless, the two-layer mantle convection regime proposed based on geochemical data (e.g., Hofmann, 1997) is hard to reconcile with geophysical observations for whole-mantle convection (van der Hilst et al., 1997). Alternatively, a ubiquitous distribution of small- to moderate-scale heterogeneity in the upper mantle is considered to be responsible for geochemical variability of MORBs and OIBs (Castillo et al., 2010; Meibom and Anderson, 2004).

The South China Sea (SCS), one of the marginal basins in the western Pacific, formed by seafloor spreading between 33 – 15 Ma (Li et al., 2014). During the period of SCS seafloor spreading, magmatic activity primarily occurred in the SCS basin and southeast China, then, after cessation of SCS seafloor spreading, intraplate volcanism was widely distributed in the SCS basin and adjacent areas (such as southeast (SE) China, the Pearl River basin, and Indochina; Fig. 1) (Wang et al., 2013; Zou and Fan, 2010). Previous studies show remarkable differences between the geochemical compositions of the spreading stage MORBs and post-spreading seamount lavas (Qian et al., 2021). However, the causes of these remain unclear. In addition, it remains unclear why volcanism after the cessation of spreading is widespread in the SCS and surrounding areas.

Although bulk-rock geochemistry of mafic volcanic rocks is commonly used to evaluate the geochemical heterogeneity of the mantle, most magmas that reach the surface represent complex mixtures of melts, which through their homogenization and re-equilibration with the surrounding mantle at shallower depths effectively erase much of their original source heterogeneity

(Kamenetsky et al., 1997; Kent, 2008; Peate et al., 2012). Detailed studies of individual rock samples, especially of the isotopic composition of their various constituents, including crystal cargo and melt inclusions trapped in the crystals, can be used to assess the heterogeneity of the underlying mantle source (e.g., Hanyu et al., 2019; Jackson and Hart, 2006; Kamenetsky et al., 1997; Kent, 2008; Qian et al., 2017; Ramos and Tepley III, 2008; Rose-Koga et al., 2017; Sobolev et al., 2011). In this study we examine the age and geochemistry (whole rock; matrix glass; olivine (ol), clinopyroxene (cpx) and plagioclase (plag) crystal; and ol and plag-hosted melt inclusion compositions) of the lavas from the syn-spreading Shixingbei seamount, and post-spreading Zhenbei-Huangyan seamount chain in the SCS (Fig. 1). Our results display considerably larger isotopic variability than observed previously from whole rocks analyses, pointing to mantle source heterogeneity beneath the SCS resulting from recycling of oceanic crust and sediments. The enriched mantle reservoirs are most likely introduced from the mantle transition zone (MTZ) into the upper mantle. Based on the temporal-spatial evolution of volcanism and our new geochemical and geophysical evidence, we propose that the Cenozoic magmatism in SE Asia is generated by active upwelling of mantle material linked to curved subduction systems.

2. Geological setting and samples

The SCS is one of the largest marginal seas in the western Pacific (~3,500,000 km^2), with the Eurasian plate to the north, the Philippine Sea plate to the east, the Australian plate to the south, and the Indian plate (or Indochina block) to the west (Fig. 1). The SCS developed as a result of multiple episodes of continental rifting and seafloor spreading during the Cenozoic (Briais et al., 1993; Li et al., 2014; Sibuet et al., 2016). The deep-water basin of the SCS comprises three parts, the East Sub-basin (ESB), Southwest Sub-basin (SWSB) and Northwest Sub-basin (NWSB) (Fig. 1). Constrained by mapping magnetic anomalies and cores recovered from the International Ocean Discovery Program (IODP) Expedition 349 (microfossil age constraints), seafloor spreading started at c. 33 Ma near the northern continental margin of the SCS (corresponding to the oldest seafloor spreading magnetic anomaly C12), and ceased at c. 15 Ma in the ESB and c. 16 Ma in the SWSB (Li et al., 2014). Late Cenozoic volcanism is widespread and a prominent feature in SE Asia (including SCS, SE China, and Indochina Peninsula), with the majority of magmatism younger than sea-floor spreading in the SCS (between c. 33 and 16 Ma) (e.g., Hoang and Flower, 1998; Wang et al., 2013; Yan et al., 2018; Zou and Fan, 2010). The SCS and nearby areas are surrounded by several subduction zones (Fig. 1), indicating that the volcanism in SE Asia took place in the same tectonic setting. In addition, the SCS post-spreading seamount lavas and synchronous intraplate lavas in SE China and Indochina Peninsula share similar chemical and isotopic characteristics with typical E-MORB to OIB-type incompatible element distributions, and distinctive Pb isotope compositions similar to EMII-type OIB (e.g., Hoang and Flower, 1998; Qian et al., 2021; Wang et al., 2013; Yan et al., 2018; Zou and Fan, 2010), suggesting a common mantle source.

The SCS preserves both seafloor spreading and post-spreading volcanic features. Seafloor spreading stage seamounts are mostly distributed in the northern SCS; post-spreading stage volcanism is more extensive in the SCS basin and predominantly occurs in ESB and SWSB, for example two north-south trending seamount chains (Longbei and Longnan seamounts; Nanyue and Beiyue seamounts) in the SWSB, and an east-west trending Zhenbei-Huangyan seamount chain in ESB. The samples for this study were collected from Shixingbei seamount, which is not in a chain, and the Zhenbei-Huangyan seamount chain in the SCS (Fig. 1) with the ROPOS remotely operated subsea vehicle operated by the Canadian Scientific Submersible Facility (Fig. S1). Shixingbei seamount lies in the middle of the SCS Basin (Fig. 1). The Zhenbei and Huangyan seamounts formed after seafloor spreading ceased in the ESB and are aligned northeastwards from the fossil spreading ridge (Li et al., 2014) (Fig. 1). Most lavas from these seamounts display pillow structures with columnar jointing (Fig. S1c and d). The basalts from the SCS seamounts are typically variably vesicular and porphyritic (3-20 %) with phenocrysts dominated by ol, cpx and plag (Fig. S2a, b, c, d, e). In some samples, ol crystals contain spinels (Fig. S2a, b), and ol and plag crystals also contain melt inclusions up to 140 μm in size (Fig. S2c, e). Biotite is found in rare evolved samples (such as trachytes), in which alkali-feldspar and cpx dominate the phenocryst assemblage (Fig. S2f).

3. Analytical methods

Complete description of the analytical techniques can be found in the supplementary material and is briefly discussed here. Plag separates from two samples (2061-R7 from Shixingbei seamount and 2055-R12 from Huangyan seamount) were selected for Ar-Ar age determinations by an ARGUS-VI multi-collector instrument at the Argon geochronology laboratory of the Oregon State University.

A U-Pb age on zircon from trachyte 2059-R16 from Zhenbei seamount was dated using a Thermo Element XR instrument connected to a RESOlution M-50 laser at Guangzhou Institute of Geochemistry, Chinese Academy of Science (GIG-CAS). Major and trace elements of the SCS seamount whole-rock samples were analyzed using a PANalytical AXIOS-Advanced X-ray fluorescence spectrometer at the State Key Laboratory of Marine Geology (SKLMG) in Tongji University, and an Agilent 7900 inductively coupled plasma-mass spectrometer (ICP-MS) at GIG-CAS, respectively. The whole-rock Sr–Nd-Pb isotopes of volcanic samples were analyzed using a Neptune Plus multi-collector (MC-)ICP-MS at GIG-CAS. Major and trace elements of minerals and glasses (matrix glass and melt inclusion) were analyzed using a JEOL JXA-8230 electron probe micro-analyzer at SKLMG in Tongji University and an excimer 193 nm laser ablation system (RESOlution M-50) coupled to a Thermo Element ICP-MS instrument at GIG-CAS, respectively. In situ Sr-Pb isotopes of feldspar, matrix glass and melt inclusion were analyzed using a Neptune Plus MC-ICP-MS with a RESOlution M-50 laser at GIG-CAS.

4. Results

4.1. Geochronology

Some samples described here were collected from Shixingbei seamount (Fig. 1), and the age of volcanism at these sites was unknown prior to this study. Plag in volcanic rock sample 2061-R7 from the Shixingbei seamount yield a $^{40}Ar/^{39}Ar$ plateau age of 19.10 ± 0.78 Ma (Fig. 2A), indicating the off-axis Shixingbei seamount formed during the syn-spreading stage (33 – 16 Ma) of the SCS. The two lavas from the Huangyan and Zhenbei seamounts in the SCS ESB yield significantly younger ages. Sample 2055-R12 from the Huangyan seamount gives a $^{40}Ar/^{39}Ar$ plateau age of 7.78 ± 0.21 Ma (Fig. 2B), which affirms a previously published K-Ar age data (7.77 ± 0.49 Ma) for samples from the same seamount (Wang et al., 2009). U–Pb dating of zircon grains from the Zhenbei seamount trachyte 2059-R16 yields a weighted mean $^{206}Pb/^{238}U$ age of 7.76 ± 0.13 Ma (n = 31; Fig. 2C). The Zhenbei-Huangyan seamount chain samples are nearly age-synchronous and do not show clear age progression. Thus, the available data indicate that the Shixingbei seamount formed while seafloor spreading was still active in the SCS, whereas the Zhenbei-Huangyan seamount lavas formed after spreading ceased.

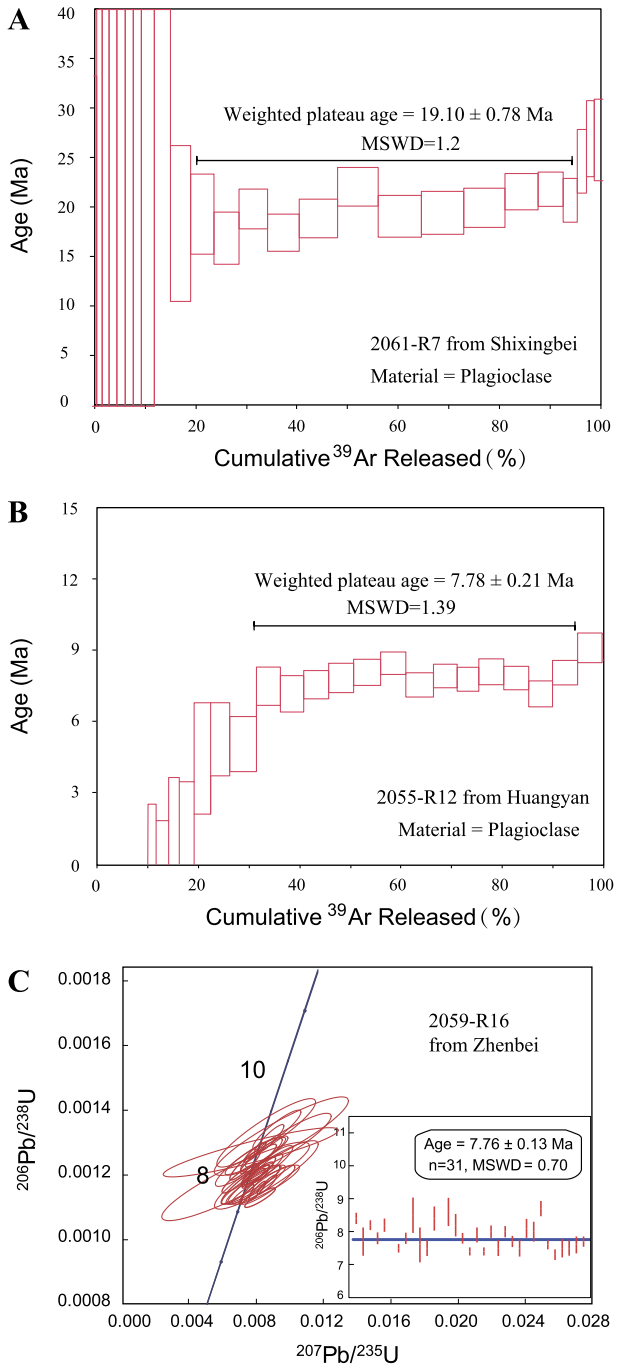

Fig. 2. The ages of the South China Sea seamount lava samples. (A-B) ^{40}Ar/^{39}Ar age spectrum for plagioclase from the Shixingbei and Huangyan seamount lavas. (C) U-Pb zircon concordia plot for sample 2059-R16 from Zhebei seamount. Inset is the weighted average of zircon ^{206}Pb/^{238}U ages.

4.2. Geochemistry

The studied Shixingbei seamount and Zhenbei-Huangyan seamount chain lavas show temporal variations in geochemical compositions. The Shixingbei seamount lavas formed during the SCS spreading stage are tholeiitic basalts (alkalis ($Na_2O + K_2O$) = 3.03 – 3.59; SiO_2 = 49.59 – 51.32; MgO = 4.90 – 5.93; all oxide contents in weight % normalized to 100% on volatile-free basis), and possess similar major element compositions to spreading stage MORBs sampled by IODP Expedition 349 within the SCS basin (Fig. 3).

The post-spreading Zhenbei-Huangyan seamount lavas range from alkali basalt through trachyte (SiO_2 = 45.2 – 62.7; MgO = 9.6 – 0.7) to basanite (SiO_2 = 43.4 – 44.4; MgO = 10.4 – 11.8) (Fig. 3). MgO is highest in ol-hosted melt inclusions (7.2 – 11.9), intermediate in plag-hosted melt inclusions (4.5 – 6.3) and lowest in matrix glass (2.2 – 4.6) (Fig. 3B). As MgO decreases in ol-hosted melt inclusions, whole rocks and matrix glass with MgO > 4.5, both SiO_2, and Al_2O_3 increase and FeO^t (t = total) decrease overall (Fig. 3), reflecting an assemblage dominated by ol, cpx and Fe-oxide fractionation. Plag melt inclusions and matrix glass with MgO < 4.5 (Fig. 3), however, are shifted to lower Al_2O_3 and Na_2O and higher FeO^t, consistent with plag joining the fractionating phases. Ol have relatively high CaO (0.16 – 0.35 wt.%) (Table S5), favoring crystallization from mafic melts rather than being xenocrysts from mantle peridotite (Qian et al., 2021). Cpx have diopsidic to augitic compositions ($En_{35-44}Fs_{11-20}Wo_{41-48}$) with relatively high Mg# (100Mg/(Mg + Fe^{+2}) = 63 – 80; Table S3). Plag range from bytownite to andesine (An_{57-75}; Table S4).

The Zhenbei-Huangyan seamount whole rock lavas, matrix glass and plag-hosted melt inclusions have incompatible element contents characteristic of intraplate volcanic rocks, showing overall enrichment in highly to moderately incompatible elements, slight relative Nb enrichment and relative K and Pb depletion (Fig. 4A, B). Notably, the SCS Shixingbei seamount tholeiitic basalts have significantly lower incompatible trace element concentrations than the Zhenbei-Huangyan seamount lavas (Fig. 4A), but slightly higher incompatible trace element concentrations than MORBs erupted during the SCS spreading stage (Fig. 4A). They also have lower La/Sm, Sm/Yb, and Nb/Zr than the Zhenbei-Huangyan seamount lavas (Fig. 4C, D).

The Shixingbei tholeiitic basalts (n = 4) formed during the SCS spreading stage have less radiogenic ^{87}Sr/^{86}Sr (0.7033 – 0.7034) and ^{206}Pb/^{204}Pb (18.537 – 18.571), and more radiogenic ε_{Nd} (5.2 – 5.4) than the Zhenbei-Huangyan lavas (^{87}Sr/^{86}Sr = 0.7035 – 0.7043, ^{206}Pb/^{204}Pb = 18.591 – 18.809, and ε_{Nd} = 3.2 – 4.8) (Fig. 5). In general, matrix glass (^{87}Sr/^{86}Sr = 0.7036 – 0.7039; ^{207}Pb/^{206}Pb = 0.832 – 0.838; ^{208}Pb/^{206}Pb = 2.092 – 2.098) and plag (^{87}Sr/^{86}Sr = 0.7035 – 0.7041; ^{207}Pb/^{206}Pb = 0.828 – 0.843; ^{208}Pb/^{206}Pb = 2.054 – 2.111) within the Zhenbei-Huangyan seamounts show a similar range of Sr-Pb isotope compositions as those exhibited by the whole rocks (^{87}Sr/^{86}Sr = 0.7035 – 0.7043; ^{207}Pb/^{206}Pb = 0.831 – 0.838; ^{208}Pb/^{206}Pb = 2.079 – 2.090) (Fig. 6; Table S1, S2 and S4). Plag-hosted melt inclusions extend to much more radiogenic Sr (^{87}Sr/^{86}Sr = 0.7037 – 0.7067) (Fig. 6; Table S2). Ol-hosted melt inclusions extend to considerably more radiogenic Sr (^{87}Sr/^{86}Sr = 0.7028 – 0.7062) and Pb (^{207}Pb/^{206}Pb = 0.778 – 0.856; ^{208}Pb/^{206}Pb = 1.959 – 2.099) isotopes (Fig. 6; Table S2). The melt inclusions in the most forsteritic ol (Fo_{88-89}) have more radiogenic Pb isotope ratios (^{207}Pb/^{206}Pb = 0.778 – 0.807; ^{208}Pb/^{206}Pb = 1.958 – 2.035) than melt inclusions in Fo_{82-87} ol (^{207}Pb/^{206}Pb = 0.816 – 0.856; ^{208}Pb/^{206}Pb = 2.050 – 2.099) (Table S2). Two melt inclusions in the same ol crystal have different ^{87}Sr/^{86}Sr (0.70581 for 2055-R7-28MI1, 0.70658 for 2055-R7-28MI2) (Tables S2).

5. Discussion

5.1. A three component mixing model for SCS seamount lava genesis

The SCS seamount lavas have a large range in Pb, Sr and Nd isotope compositions (Fig. 5). It is critical to determine if this isotopic variability reflects a heterogeneous source, or whether crustal contamination during magma ascent and emplacement has modified the isotopic signal. Since ^{87}Sr/^{86}Sr ratios in 6 – 15 Ma oceanic crust (e.g. IODP sites 504 and 1256) (Höfig et al., 2014) generally do not exceed 0.7040 (only ~5%), assimilation of in-situ altered oceanic

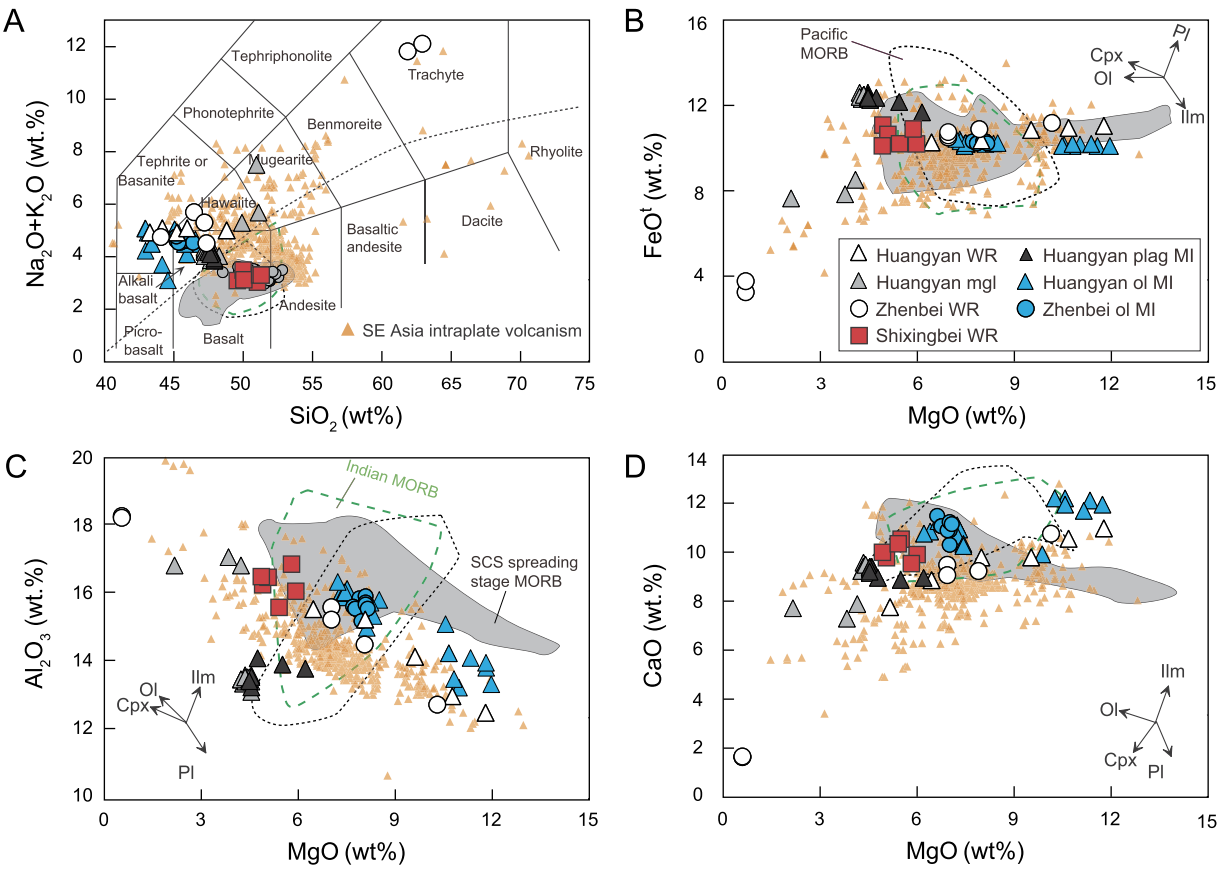

Fig. 3. Variation of major elements in whole rocks, melt inclusions and matrix glasses for South China Sea (SCS) seamount lavas. (A) SiO_2 versus (vs.) total alkali (Na_2O + K_2O) content, MgO vs. (B) FeO^t, (C) Al_2O_3, and (D) CaO for whole rocks (WR), matrix glasses (mgl), and olivine (ol)-hosted and plagioclase (plag)-hosted melt inclusions (MI) from Shixingbei, Huangyan and Zhenbei seamounts. Data of spreading stage MORB and post-spreading lavas in the SCS and intraplate volcanism in surrounding area (e.g. Southeast China, Taiwan and Indochina) are from the GEOROC (http://georoc.mpchmainz.gwdg.de/georoc). Mineral abbreviations cpx and ilm denote clinopyroxene and ilmenite, respectively.

crust is unlikely to generate the radiogenic $^{87}Sr/^{86}Sr$ (extending to 0.7067) observed for lavas from the SCS and surrounding areas. Sediment assimilation is also unlikely due to the paucity of sediment (< 10 m) on the seafloor at the time the seamounts formed (Li et al., 2014). It is noteworthy that the isotope systematics of most of these lavas do not appear to be significantly affected by crustal assimilation, as suggested by isotope ratios being mostly independent of the degree of differentiation (e.g. MgO, Mg/Si, Mg# and/or Fo content) (Fig. S6). In addition, the SCS seamount lava and most intraplate lava samples with high-ε_{Nd} (> 2.7) from SE Asia have a large variation in Nb/U with no correlations with ε_{Nd}, indicating insignificant crustal contamination (Fig. S6). By contrast, the low-ε_{Nd} (< 2.7) lavas (mainly from the Indochina Peninsula; Wang et al., 2013) show strong covariation between Mg/Si, Nb/U, and ε_{Nd} (Fig. S6), indicating that they are most likely affected by crustal contamination.

Lava whole rock compositions are commonly assumed to represent melt compositions (possibly, except for melt volatile element compositions), implying that minerals crystallized from that melt should inherit the whole rock composition. This assumption, however, is not valid for the Zhenbei-Huangyan lavas. The most mafic (MgO = 10.4 – 11.8) basanitic lavas represent complex mixtures of evolved basaltic melt (matrix glass with Mg# (100 Mg/(Mg + Fe^{2+})) = 32 – 44) and a complex crystal cargo, primarily mafic ol (Fo_{82-89}) and cpx (Mg# = 63 – 80) but also Fe oxides and plag. Plag have major element and Sr-Pb isotopic compositions compatible with being phenocrysts because their isotopic compositions are similar to those of their host whole rocks. The plag- and ol-hosted melt inclusions, on the other hand, show a large variation in Sr isotopes and record interaction with an EMII-like component with radiogenic $^{87}Sr/^{86}Sr$ (≥ 0.7067) (Fig. 6). In addition, the plag- and ol- melt inclusions have higher MgO contents and show larger variations in isotopic compositions compared to the matrix glasses (Fig. 3, 6). Ol, thus, must have crystallized from more mafic melts than the matrix glasses (Fig. 3, 6).

Whole rock Sr-Nd-Pb isotope compositions of post-spreading lavas from the SCS and nearby areas (SE China and Indochina) (Fig. 5) have previously been explained by mixing of at least two major components: depleted upper mantle or the SCS spreading lavas and an EMII-like component (Wang et al., 2013; Zou and Fan, 2010). However, this two-component mixing model does not adequately explain the isotope compositions of ol and plag-hosted melt inclusions from Zhenbei-Huangyan seamounts (Fig. 6). Instead, they require mixing of at least three distinct components (Fig. 6):

1) DMM: Zhenbei ol-hosted (Fo_{83-84}) melt inclusions and IODP Site U1431 MORB lavas (Zhang et al., 2018) have non-radiogenic Sr ($^{87}Sr/^{86}Sr \leq 0.7029$) and moderately radiogenic Pb ($^{207}Pb/^{206}Pb > 0.86$; $^{208}Pb/^{206}Pb \geq 2.10$) isotopes, characteristic of a depleted upper mantle MORB type source;

2) FOZO: Huangyan melt inclusions hosted in magnesium-rich ol (Fo_{88-89}) in equilibrium with mantle peridotite have non-radiogenic Sr ($^{87}Sr/^{86}Sr$ = 0.7036 – 0.7037) and radiogenic Pb ($^{207}Pb/^{206}Pb$ = 0.78 – 0.81; $^{208}Pb/^{206}Pb$ = 1.96 – 2.03) isotopes. They are similar to the FOZO component ubiquitous in mid-ocean-ridge and intraplate basalts (Hanan and Graham, 1996; Stracke et al., 2005);

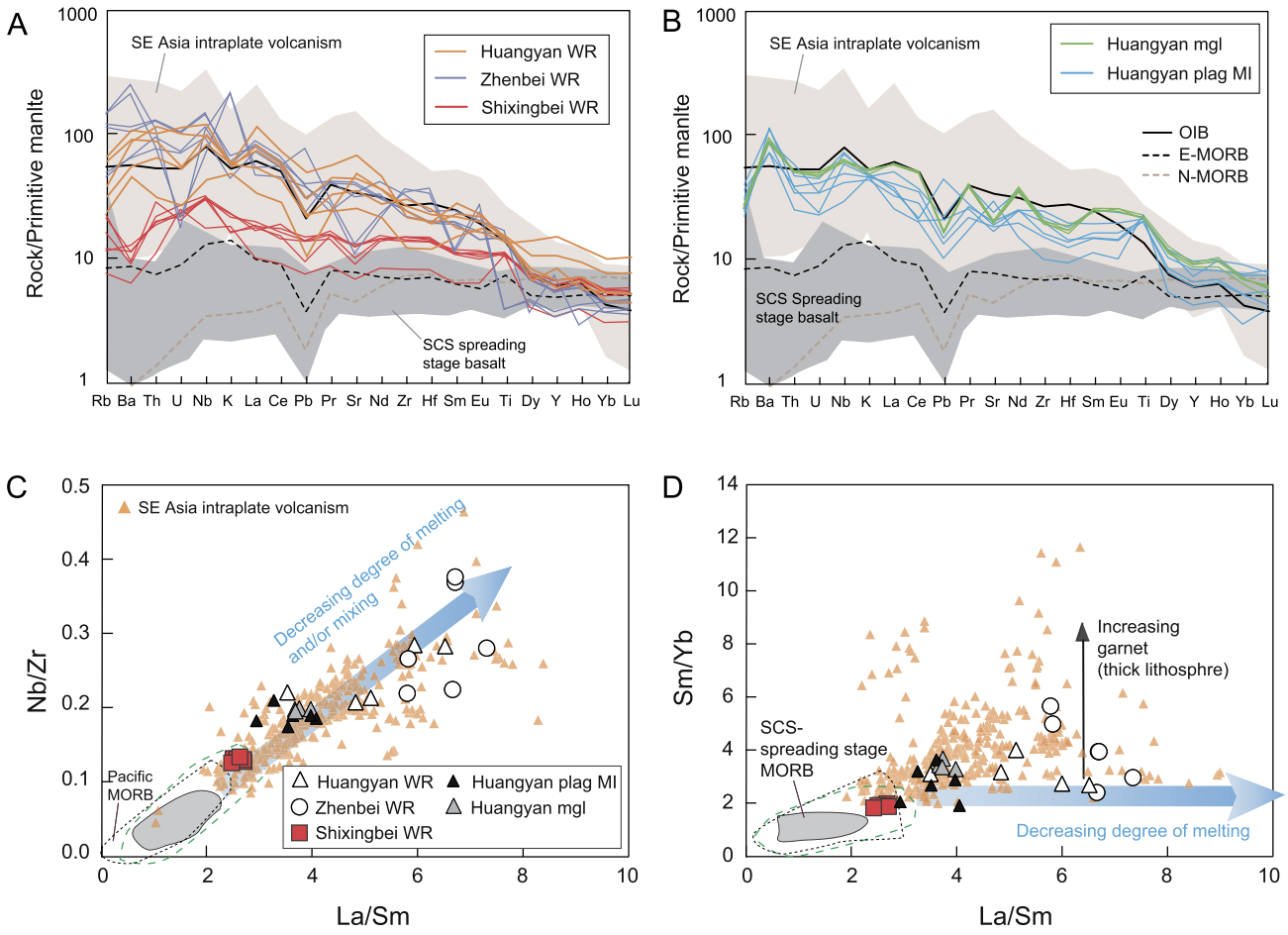

Fig. 4. Variation of trace elements in whole rocks, melt inclusions and matrix glasses for South China Sea (SCS) seamount lavas. (A-B) Incompatible multi-element diagrams, (C) Nb/Zr vs. La/Sm, (D) Sm/Yb vs. La/Sm for whole rocks (WR) from Shixingbei, Huangyan and Zhenbei seamounts, and matrix glass and melt inclusion from Huangyan lavas. Trace element data of primitive mantle, N-MORB, E-MORB and OIB are from Sun and McDonough (1989). The SCS spreading stage MORBs (Zhang et al., 2018), and Pacific and Indian MORBs (Gale et al., 2013) are shown for comparisons. Data source of intraplate volcanism in southeast (SE) Asia is the same as in Fig. 3. To minimize the effect of crustal contamination, intraplate lavas in SE Asia with $\varepsilon_{Nd} < 2.7$ have been excluded.

3) EMII: Huangyan melt inclusions hosted in plag and some ol (at least three ol crystals) require a component with the most radiogenic Sr ($^{87}Sr/^{86}Sr \geq 0.7067$) and moderately radiogenic Pb ($^{207}Pb/^{206}Pb = 0.826 - 0.845$; $^{208}Pb/^{206}Pb = 2.06 - 2.10$) isotopes.

Clearly, plag and ol crystals crystallizing from the same magma batch should possess identical isotopic compositions, therefore the large range of plag- and ol-hosted melt inclusions compositions seen in the SCS seamount lavas (i.e. Fig. 6) requires trapping melts of isotopically distinct parental magmas (Qian et al., 2017; Ramos and Tepley III, 2008; Rose-Koga et al., 2017). The FOZO-like signature in particular is only clearly identified in a few ol-hosted melt inclusions, implying that the proportion of the FOZO component contributing to erupted lavas must be small, and/or that the FOZO-like fragments in the mantle are so small that they are rarely sampled in melt inclusions. They are probably present in the whole rock, but they are so diluted that the FOZO "flavor" cannot be distinguished. It is apparent that shallow-level storage and magma mixing resulted in dilution of the FOZO component in the SCS seamount lavas, before eruption.

5.2. Rapid recycling of slab-derived source components

We now discuss the possible origin of the enriched components (EMII and FOZO) necessary to explain the isotopic variations of the crystals and their MIs in the SCS (Fig. 6). Some plag- and ol-hosted melt inclusions have more radiogenic $^{87}Sr/^{86}Sr$ than matrix glasses and plag crystals, and form mixing arrays between SCS-spreading or Pacific MORBs and EMII (Fig. 6).

Subducting marine sediment, seawater-altered ocean crust and EMII have similar Pb isotope compositions but can extend to more radiogenic $^{87}Sr/^{86}Sr$ and could serve as this end member (Fig. 6). Compared to matrix glass, plag-hosted melt inclusions extend to lower (Ce, Nd)/Pb but higher Ba/La ratios (Table S2), also favoring sediments as the EMII component. Geophysical studies provide additional support for recycled oceanic crust components beneath the SCS and Indochina. They could originate from subducted Neo-Tethyan slabs from the southwest (230 – 90 Ma) (Chung et al., 2005), or paleo-Pacific and Pacific slabs from the east (300 – 120 Ma) (Li and Li, 2007). Given that the SE China region was far from the Neo-Tethyan tectonic realm during the Mesozoic, it is likely that recycled Neo-Tethyan slabs are not the major source of the FOZO-like signature observed in Cenozoic lavas.

The observed Sr and Pb isotopic heterogeneity in young (130-170 Ma) Pacific oceanic crust and marine sediments from ODP sites 801 and 1149, east of the Mariana and Izu-Bonin arcs (Hauff et al., 2003), respectively, covers the entire range exhibited by SCS spreading MORB, post-spreading volcanism and their crystal cargoes and melt inclusions, and even extends to more extreme compositions (Fig. 6). For the purpose of our modeling, we considered Pacific MORB from site 801C with high μ ($^{238}U/^{204}Pb = 51$) and radiogenic Pb ($^{206}Pb/^{204}Pb = 20.03$; $^{207}Pb/^{206}Pb = 0.777$; $^{208}Pb/^{206}Pb = 1.881$; Hauff et al., 2003) as the FOZO component

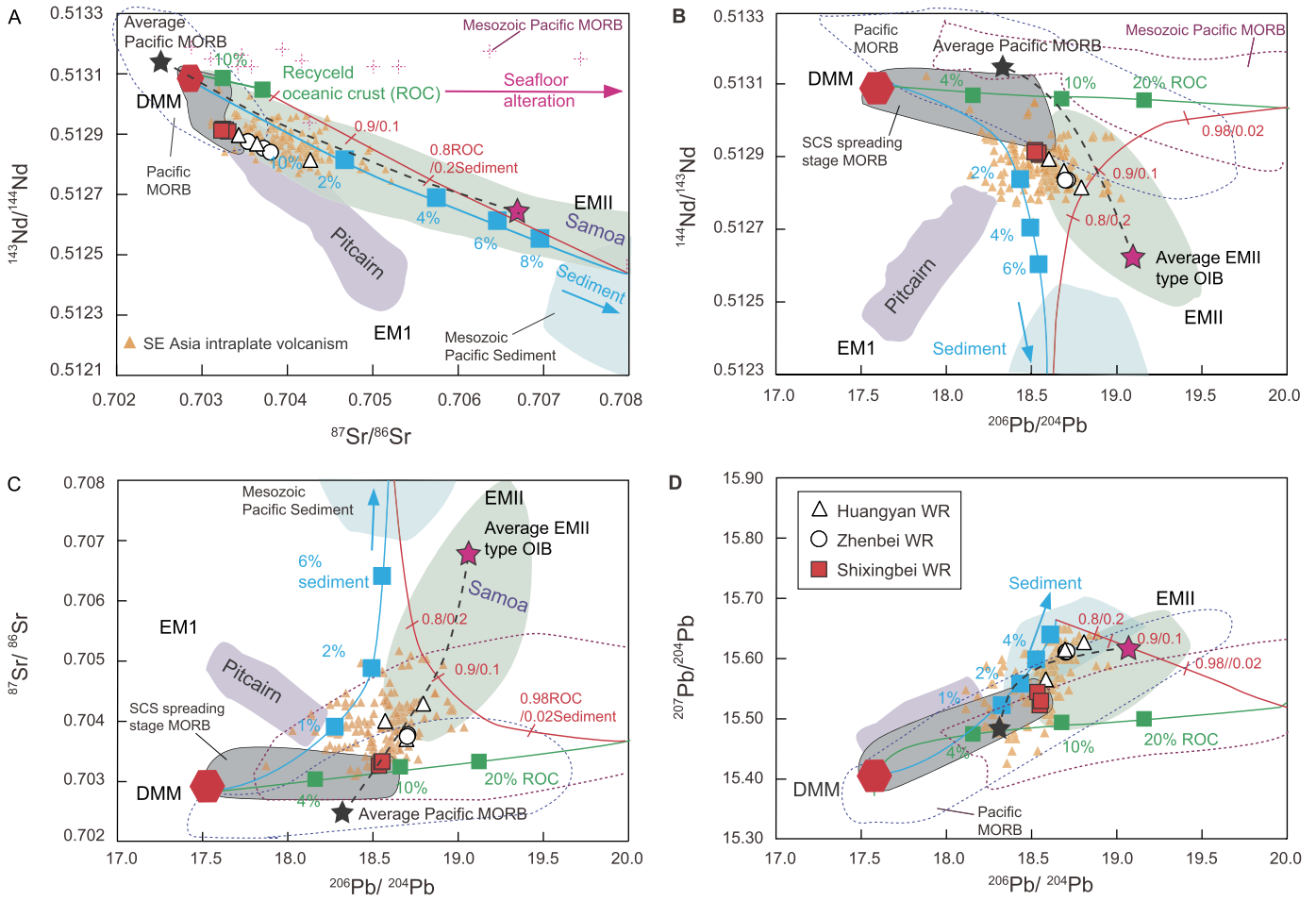

Fig. 5. Isotopic characteristics of the South China Sea (SCS) seamount samples. (A) $^{87}Sr/^{86}Sr$ vs. $^{143}Nd/^{143}Nd$, (B) $^{143}Nd/^{143}Nd$ vs. $^{206}Pb/^{204}Pb$, (C) $^{87}Sr/^{86}Sr$ vs. $^{206}Pb/^{204}Pb$, (D) $^{207}Pb/^{204}Pb$ vs. $^{206}Pb/^{204}Pb$ for whole rocks (WR) from Shixingbei, Huangyan and Zhenbei seamounts. Data sources: the SCS spreading stage MORBs (Zhang et al., 2018); Pacific MORBs, EMI-type and EMII-type oceanic island basalts (Stracke et al., 2003), and intraplate lavas in the SCS and SE Asia from the GEOROC database (http://georoc.mpchmainz.gwdg.de/georoc). The modeling results show mixing trends (solid lines) between depleted SCS MORB mantle end-component (DMM) and recycled oceanic crust and sediments. Dashed lines show mixing between averaged Pacific MORB, and typical EMII mantle derived partial melt. To minimize the effect of crustal contamination, intraplate lavas in southeast Asia with $\varepsilon_{Nd} < 2.7$ have been excluded. The main parameters in the mixing model are given in Supplementary Table S9.

(Hanan and Graham, 1996; Stracke et al., 2005). Marine sediments (clay, chert and nannofossil marl) from Sites 801 and 1149 in Pacific Ocean with very radiogenic Sr ($^{87}Sr/^{86}Sr = 0.70954$) and relatively radiogenic Pb ($^{206}Pb/^{204}Pb = 18.61$, $^{207}Pb/^{206}Pb = 0.845$, and $^{208}Pb/^{206}Pb = 2.089$) (Hauff et al., 2003) as the EMII component. Our isotope modeling results (Fig. 5 and 6) show that the isotopic heterogeneity seen in the SCS spreading- and post-spreading lavas could represent mixtures of depleted upper mantle with recycled oceanic crust and sediment.

The FOZO component ubiquitous in mid-ocean-ridge and intraplate basalts was proposed to represent young ocean crust recycled through the transition zone and/or upper mantle (Hanan and Graham, 1996; Stracke et al., 2005). Since the SCS lavas have $^{3}He/^{4}He$ (7.4 – 8.0 R/R_A) similar to or lower than MORB (Qian et al., 2021), the MTZ is the most likely storage location for ocean crust evolving to FOZO (Hanan and Graham, 1996). Here we use a Monte Carlo simulation (see Fig. 7, S7, and Table S11; see supplementary material for further details) to constrain the possible combinations of source maturation times (in Ma) and μ ($^{238}U/^{204}Pb$) values required to reproduce the FOZO-like Pb isotope signature seen in the SCS. The Monte Carlo simulation (Fig. 7, S7 and Table S11) randomly chooses an initial Pb isotope compositions and a μ value, which falls within the range seen in typical unradiogenic paleo-Pacific oceanic crust, then calculates the time required to evolve to the FOZO endmember. Pb isotope compositions always take longer to evolve with a lower μ, but all scenarios are consistent with the relatively short timescales (< 500 Myr) needed to generate the required FOZO-like isotope signature (Fig. 7). Based on the average μ of 42 measured in Pacific oceanic crust all the potential initial compositions can reproduce the FOZO-like component in less than 120 – 350 Myr (Fig. 7). Thus, on the basis of the unique geochemical constraints and geological setting, it seems most plausible that the MTZ beneath SE Asia was most likely enriched by subducted materials from past paleo-Pacific plate subduction. Given that the subduction of the paleo-Pacific plate beneath SE Asia took place between c. 250 and 150 Ma (Li and Li, 2007), the timescales for oceanic crust recycling in marginal sea basin (e.g., < c. 250 Ma) are significantly shorter than those associated with the deep plate subduction and mantle plume upwelling (possibly > 1.0 Gyr) (Chase, 1981; Hanyu et al., 2019; Stracke et al., 2003). It has previously been shown that the Pb isotopic composition of FOZO can be generated from 300 Ma-age oceanic crust, if some Pb from a continental source (e.g. pelagic sediments) was added during hydrothermal alteration shortly after crust formation (Hanan and Graham, 1996). In particular, given that the abundant seamount lavas or OIBs formed during the seafloor spreading and post-spreading stage are highly variable in isotopic composition, their subduction and recycling could be a plausible process to pro-

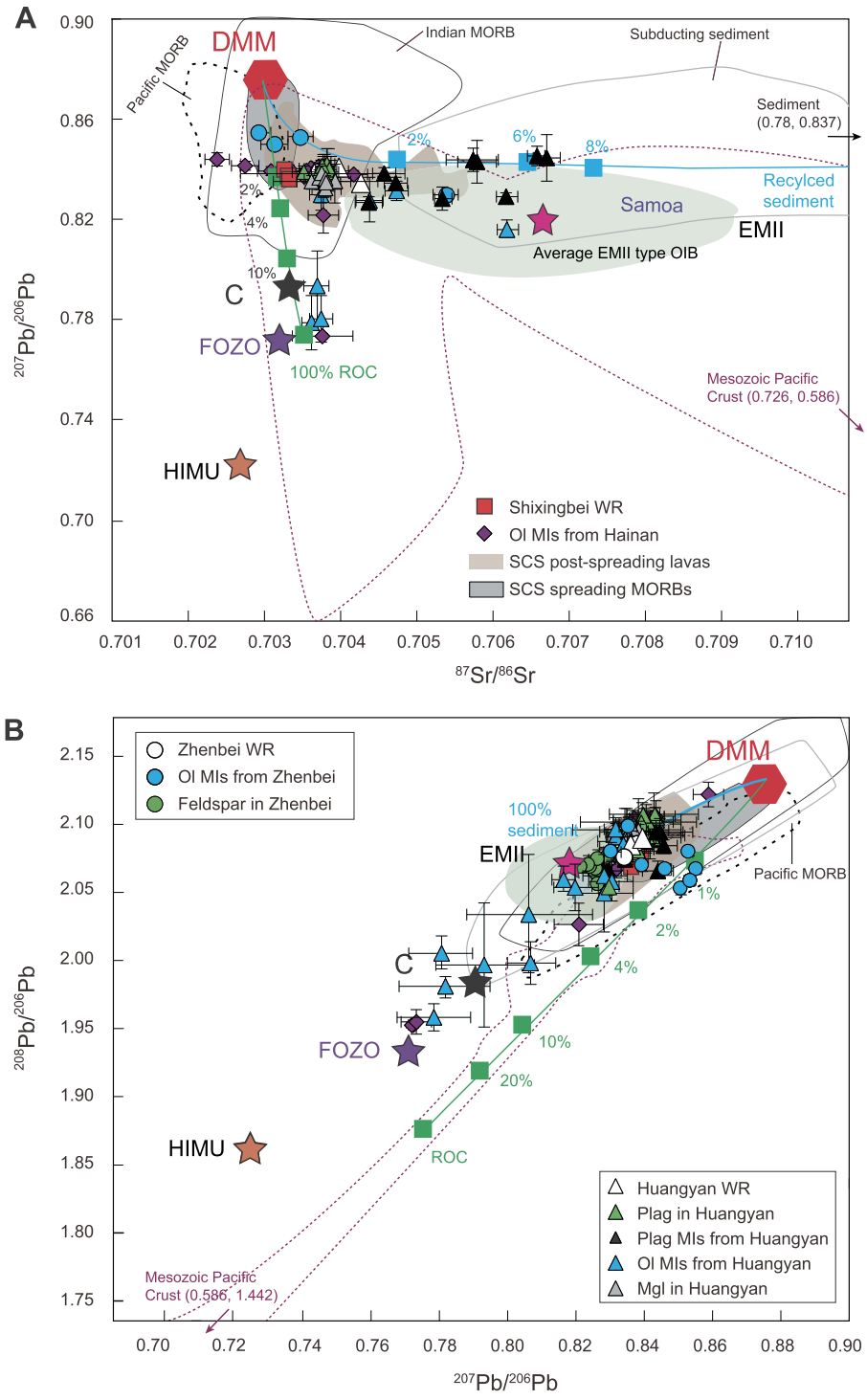

Fig. 6. Isotopic variations in melt inclusions, whole rocks and matrix glasses for South China Sea (SCS) seamount lavas. (A) $^{87}Sr/^{86}Sr$ vs. $^{207}Pb/^{206}Pb$ and (B) $^{207}Pb/^{206}Pb$ vs. $^{208}Pb/^{206}Pb$ isotope diagram for whole rocks from Shixingbei seamount lavas, and whole rocks (WR), matrix glass (mgl), olivine (ol)-hosted and plagioclase (plag)-hosted melt inclusions (MI) and feldspars from Huangyan and Zhenbei seamount lavas, illustrating that at least three components are required to explain the observed variations in isotopic composition: DMM-depleted SCS MORB-source upper mantle, represented by the most depleted SCS MORB (Zhang et al., 2018), FOZO-type component, interpreted as reflecting the young recycled material in the mantle transition zone (Hanan and Graham, 1996; Stracke et al., 2005), well represented by young recycled Mesozoic Pacific MORB (Hauff et al., 2003), and an EMII-type component – represented by Mesozoic Pacific Ocean sediment (Hauff et al., 2003). The main parameters in the three-component-mixing model between DMM and recycled oceanic crust and sediments are the same as in Fig. 5. Data sources: unpublished data from ol-hosted melt inclusions from Hainan island lavas, to the north of the SCS, from Mei (2018); the SCS post-spreading lavas, and Pacific and Indian MORB (http://georoc.mpch-mainz.gwdg.de/georoc/); U1431 SCS spreading stage MORBs (Zhang et al., 2018); Mesozoic Pacific ocean crust (Hauff et al., 2003); EMII (typical EM-2 OIBs), and HIMU (typical HIMU OIBs) end members (Stracke et al., 2003); FOZO (Stracke et al., 2005) and C (Hanan and Graham, 1996). To minimize the effect of crustal contamination, intraplate lavas in southeast Asia with $\varepsilon_{Nd} < 2.7$ have been excluded.

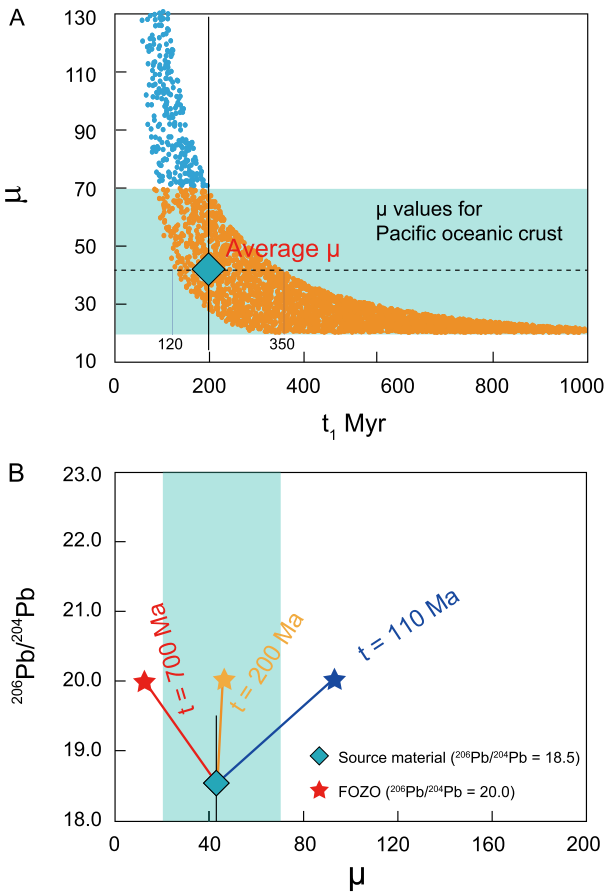

Fig. 7. Results of Monte Carlo simulations for Pb model evolution of the recycled component in FOZO mantle source. (A) Monte Carlo results derived from Equation (1) in the supplementary material for R1 values. $\mu = {}^{238}U/{}^{204}Pb$, the green area shows the range for μ values for Pacific oceanic crust and the dashed blue line defines the average μ value; (B) Modeling μ in the mantle source. Modeled μ compositions that are necessary to produce radiogenic $^{206}Pb/^{204}Pb$ of typical FOZO ($^{206}Pb/^{204}Pb = 20.03$) signature starting from an un-radiogenic sample ($^{206}Pb/^{204}Pb = 18.5$) of the paleo-Pacific oceanic crust (Hauff et al., 2003). Each line corresponds to possible source ages and the necessary μ for that source to generate the radiogenic $^{206}Pb/^{204}Pb$ of typical FOZO lavas.

duce enriched MORB or intraplate lavas isotopic signatures over relatively short timescales. The MTZ has been proposed as the most likely storage location for such young ocean crust evolving to these FOZO-like intermediate compositions (Hanan and Graham, 1996; Stracke et al., 2005). Thus, recycling of ocean crust through the upper mantle and transition zone can occur on relatively short time scales. This rapid reworking is consistent with other studies that have argued for short ($\leq$ 600 Myr) recycling times based on evidence from mid-ocean ridge and intraplate volcanism (e.g. Hoernle et al., 2011; Mazza et al., 2019; McCoy-West et al., 2016; Sobolev et al., 2011). Ultimately, recycling of enriched oceanic lithosphere through the transition zone over those short time scales ($<$ 250 Myr) seen in the SCS has the potential to significantly enhance upper mantle heterogeneity.

5.3. Source heterogeneity and melting process control on geochemical variations of late Cenozoic volcanism

Our new Ar-Ar dating results show that the Shixingbei seamount is 19.10 $\pm$ 0.78 Ma (Fig. 2A), and is 3 – 5 Myr younger than the underlying MORBs, which formed around 23 – 24 Ma with a spreading rate of c. 25 km/Myr based on magnetic anomaly data (Li et al., 2014). The final age of seafloor spreading in the ESB of the SCS is estimated to be c. 15 Ma (Li et al., 2014). The Shixingbei seamount, is $\leq$ 150 km away from the present-day fossil ridge axis in the ESB (Fig. 1), indicating that it formed off-axis on the flank of the fossil ridge.

Off-axis seamounts can form near a ridge axis if an excessive magma supply is available from residual mantle upwelling feeding volcanic activity on the ridge axis. Following abandonment of a spreading ridge, the average degree of mantle melting under the abandoned ridge progressively decreases with time due to the decrease in mantle upwelling rate (seafloor spreading rate) and the increase in overlying lithosphere thickness by conductive cooling as it moves further off-axis (Brandl et al., 2012; Haase et al., 2011). This is observed in the off-axis Shixingbei seamount where the seafloor spreading rate in the SCS decreased rapidly due to a ridge jump at 25 Ma (Li et al., 2014). As off-axis seamount lavas are generated by lower degrees of melting of heterogeneous mantle they would contain a larger contribution from more fusible and enriched components, which are expected to have relatively enriched geochemical flavor (e.g., Brandl et al., 2012; Castillo et al., 2010; Haase et al., 2011). Compared to the SCS spreading stage MORBs, the off-axis Shixingbei seamount basalts have more enriched trace element (elevated La/Sm and Nb/Zr, Fig. 4) and isotopic compositions (more radiogenic Sr and less radiogenic Nd isotope signatures, Fig. 5). Thus, the off-axis Shixingbei seamounts lavas were generated by lower degrees of melting of a heterogeneous magma source relative to SCS MORBs generated at the spreading center.

The Zhengbei and Huangyan seamounts have been dated at c. 7.8 Ma (Fig. 2), which is much younger than the underlying fossil spreading ridge in the ESB of the SCS that was active at 15 Ma (Li et al., 2014). Previous studies have shown that buoyancy-induced upwelling by melt-depleted residual mantle and associated lower degree melting relative to spreading stage can be responsible for continued magmatism on fossil ridges for several Myr after active spreading ceased (Brandl et al., 2012; Castillo et al., 2010; Haase et al., 2011). A similar mechanism can explain to some extent the enriched geochemical signatures observed in some seamounts on the SCS fossil ridges that erupted several Myr after spreading ceased. The post-spreading stage Huangyan and Zhenbei seamount lavas are characterized by E-MORB- to OIB-type incompatible element abundances, and compared to the spreading stage MORBs and off-axis Shixingbei seamount lavas, show a significantly higher La/Sm, fractionated HREE element patterns ($Sm/Yb \gg 1$), and more enriched Sr and Nd isotope compositions (Fig. 4, 5). This suggests that the post-spreading seamount lavas were most likely generated by lower degrees of melting with residual garnet in their mantle source. The geochemical compositions of SCS seamount lavas together with the new age data indicate that the variable degrees of melting of heterogeneous mantle can reproduce the trace element and isotope variations in the lavas.

Interestingly, similar features are observed in intraplate volcanism throughout SE Asia, there is a large contrast in the compositions of magma generated during the SCS spreading (33 – 16 Ma) and post-spreading (post-16 Ma) stages (Fig. 4, 5, 8C and D). Spatially, compared to the post-spreading seamount lavas in the SCS basin, there are significantly larger chemical and isotopic variations (e.g., Sm/Yb and $^{87}Sr/^{86}Sr$) in the intraplate basalts from neighboring areas (western- and northern-group), although this could simply reflect much less data from the SCS basin (Fig. 8E, F). The post-spreading basalts in the SCS basin erupted on thinner lithosphere (45 – 50 km) have geochemical characteristics consistent with higher degrees (F) and shallower depths (P) of melting (e.g., lower Sm/Yb; Fig. 8E), whereas intraplate basalts erupted on thicker lithosphere (60 – 90 km) (Wu et al., 2004) (e.g., south China and Indochina, north and west of the SCS) show the inverse (Fig. 8E). In accordance with these observations, we propose that there was a common mantle source beneath SE Asia during the spreading and post-spreading stages, but the enriched (OIB-

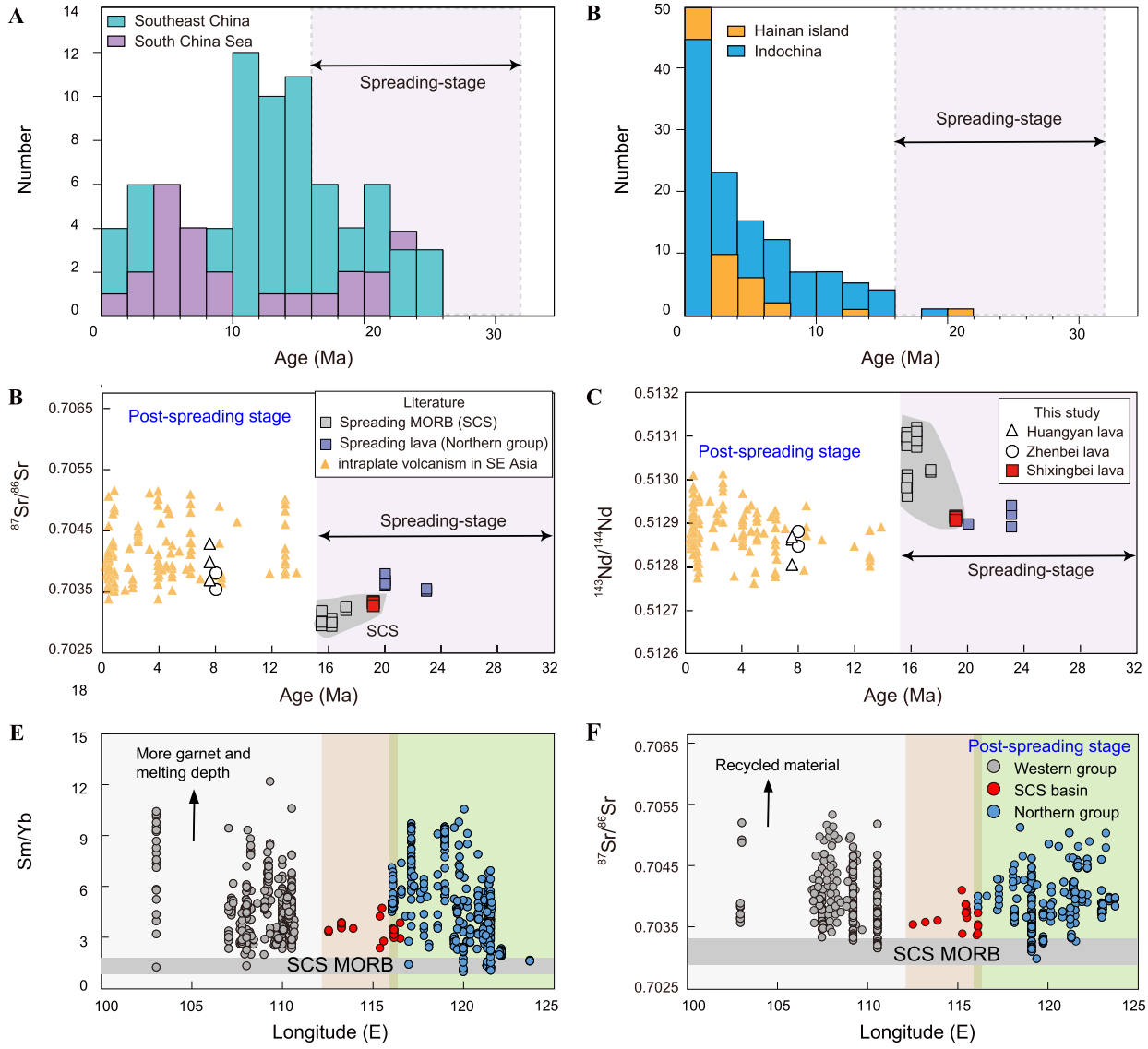

Fig. 8. Spatial and temporal evolution of Cenozoic lavas in the South China Sea (SCS) and surrounding areas. (A-B) Histogram showing age ranges for Cenozoic (spreading- and post-spreading stage) lavas in the SCS and surrounding areas. (C-D) Temporal variation of geochemical composition of spreading- and post-spreading stage lavas in the SCS and surrounding areas. (E-F) Spatial variation of geochemical composition of intraplate lavas from the SCS, western group (Indochina and Leiqiong, to the west of the SCS) and northern group (including south China and Taiwan, to the north of the SCS) shown in Fig. 1. Data for ages and compositions of Cenozoic lavas in the Southeast Asia from the GEOROC (http://georoc.mpchmainz.gwdg.de/georoc). Intraplate lavas in southeast Asia affected by crustal contamination have been excluded.

type) mantle was generally more diluted in the SCS MORBs and seamount lavas due to greater degrees of melting at shallower depths. Our new results support a model where variable degrees of melting of a heterogeneous mantle are responsible for geochemical variability of MORBs and OIBs (Meibom and Anderson, 2004).

5.4. Volcanism in SE Asia linked to subduction-induced mantle upwelling

The causes of intraplate volcanism and dynamics of mantle upwelling in SE Asia are the subject of debate, and have been variously attributed to the Hainan mantle plume (e.g. Wang et al., 2013; Yan et al., 2018; Zou and Fan, 2010), plate subduction induced mantle flow (e.g. Lin et al., 2019; Qian et al., 2021), and eastward mantle flow escape in response to Indo-Eurasian collision (e.g., Hoang and Flower, 1998). Volcanism in SE Asia is not easily explained by a model with a mantle plume rooted at the core–mantle boundary under Hainan island because: (1) multiple volcanic episodes of distinct chemistry and age are observed in SE Asia (Hoang and Flower, 1998; Fig. 1); (2) the volcanism around Hainan island is much younger and obviously weaker than that in nearby areas (SE China, SCS and Indochina) (Fig. 1); (3) $^{3}He/^{4}He$ of SCS seamount glasses (7.36 to 8.03 R/R_A) are significantly lower than classical mantle plume-derived basalts (Hawaii and Iceland) but typical of normal MORB (Qian et al., 2021); (4) there is no well-defined 'hotspot' track associated with age-progressive volcanism in SE Asia (Li et al., 2014; this study); and, (5) broad (i.e. non plume-shaped), ambiguous P-wave tomographic anomalies above the transition zone together with weaker, diminishing slow anomalies below the transition zone beneath SE Asia, challenge the view of the 'Hainan plume' as a classical plume structure (Lin et al., 2019).

The SE Asia region is surrounded by several subduction zones (Fig. 1), suggesting a potential association between plate subduction and magmatic activity (Lin et al., 2019). During the seafloor spreading stage of the SCS, in addition to formation of new oceanic crust and a small number of seamounts near the spreading center, igneous activity (with ages between 26 – 16 Ma) occurred pre-

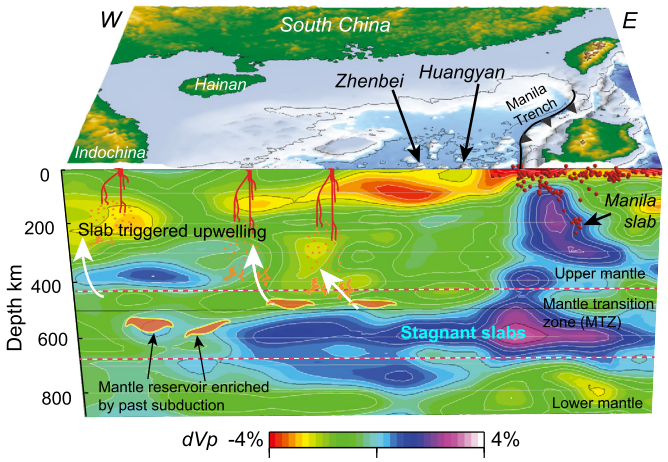

Fig. 9. Schematic model illustrating the formation mechanism of the Cenozoic volcanism in southeast Asia based on integration of seismic and geochemical data. Mantle structure beneath the South China Sea (SCS) shown by FWEA18 full waveform tomography P-wave perturbations (Tao et al., 2018) and earthquakes (red circles). Tomographic fast anomalies indicate a swath of sub-horizontal subducted oceanic lithosphere beneath the SCS at 500 – 700 km depths from previous subduction events. Although a small amount of stagnant material may be older recycled slabs from past subduction, most of the visible stagnant slab segments stored in the transition zone imaged by seismic tomography are likely to be younger subducted slabs from nearby circum-SCS subduction zones (i.e. Indo-Australian, Pacific, Philippine Sea plates, or Proto-SCS slabs). Even after SCS spreading ceased at 15 Ma, the more buoyant metasomatized mantle continues to upwell and melt to form the SCS seamounts and possibly intraplate basalts in South China and Indochina with EMII type compositions.

dominantly along coastal SE China and the SCS northern margin (see Fig. 1, 8A). Its spatial extent could indicate that the spreading stage volcanism might be induced by westward subduction of the Pacific and Philippine Sea plates beneath Eurasia, since these were located along eastern SE Asia. Intraplate magmatism within Indochina (peaking $<$ 8 Ma) is generally younger than along coastal SE China (generally 10 – 16 Ma) (Hoang and Flower, 1998; Fig. 1, 8A and B). Seismic tomography studies show evidence for the subduction of the Indo-Australian plate beneath SE Asia along the Sunda trench with slab segments deflected horizontally in the MTZ towards the SCS and Indochina (Li and van der Hilst, 2010). Therefore, it seems likely that Cenozoic volcanism in Indochina could be related to subduction-induced mantle upwelling along the Sunda trench. Hainan island is far from any subduction zones and shows intraplate volcanism peaking $<$ 5 Ma, much younger than the age of the volcanism in the SCS and coastal areas of SE China (Zou and Fan, 2010; Fig. 1, 8B). Thus, the spatiotemporal distribution and evolution of the intraplate volcanism could plausibly be active upwelling of mantle material linked to circular subduction systems of the Pacific, Philippine Sea, and Indo-Australian plates (Fig. 9). Indeed, geodynamic models that tested a variety of inputs to SE Asian plate reconstructions demonstrated robust, localized upper mantle upwellings within SE Asia during the Cenozoic that were induced by the regional subduction (Lin et al., 2019).

Here, we propose a simple conceptual model linking the flux from multiple subducting plates to upper mantle heterogeneity, and volcanism in SE Asia (Fig. 9). The induced mantle upwelling associated with local subduction can be generated ahead of a deep subducting slab and adjacent to edges of the stagnant slab segments in the transition zone, despite being far from arcs (Faccenna et al., 2010). Recent geodynamic models showed that this slab flux would stimulate upwelling of the enriched MTZ reservoirs and eventually lead to volcanic eruptions (Mather et al., 2020). We suggest that this subduction-induced upwelling originating from the MTZ and surrounding area as revealed by seismic tomography, and associated decompression melting feed the diffuse and non–age-progressive volcanism in SE Asia. A similar mantle return flow, driven by long-lived subduction, has also been proposed to cause the intraplate volcanism across eastern Australia and Zealandia, as well as northern and northeastern China (Mather et al., 2020; Zhao et al., 2011). Slab-triggered mantle return flow beneath SE Asia is significantly more complex than under eastern Australia-Zealandia and, northern and northeastern China, as SE Asia is surrounded by complicated convergent subduction systems on three sides. Therefore, it remains challenging at present to reconstruct and pinpoint the exact geochemical signature and mantle flows associated with a specific subducted slab flux. Further geodynamic modeling, high-resolution seismological studies and geochemical and age constraints on magmatism are required to quantify the link between cycling of subduction-induced mantle flows and time-space evolution of volcanism.

6. Conclusions

We present new geochemical and geochronological data for lavas from the South China Sea (SCS) seamounts. Through comparison with existing geochemical data we investigate mantle source compositions and the mantle evolution, and infer a possible mechanism to generate mantle heterogeneity and the volcanism in the SCS and surrounding areas. The major results of this work are as follows:

1. The Shixingbei seamount lavas, formed during the syn-spreading stage (19.1 Ma; 33–16 Ma), are limited to tholeiitic basalts. The Zhenbei-Huangyan seamount lavas, formed during the post-spreading stage (7.8 Ma), show wide variations in chemical compositions, ranging from basanite through alkali basalt to trachyte. The SCS Shixingbei seamount tholeiitic basalts are more depleted in incompatible trace element (e.g. La/Sm and Sm/Yb), and have less radiogenic $^{87}Sr/^{86}Sr$ and more radiogenic $^{143}Nd/^{144}Nd$ relative to most post-spreading lavas. Mantle source heterogeneity together with melting process control spatial–temporal (spreading and post-spreading stage) geochemical variations of lavas from the SCS and surrounding areas.

2. Zhenbei-Huangyan seamount whole rocks, matrix glass and plag show limited isotopic variation, while ol-hosted and plag-hosted melt inclusions show large variations in radiogenic Sr and Pb isotope ratios. A three-component mixing model (DMM-EMII-FOZO) is required to adequately explain the variability in isotopic compositions of the ol-hosted and plag-hosted melt inclusions.

3. The combined trace element and isotopic data of the SCS seamount melt inclusions, minerals and lavas demonstrate that the mantle source in the region is influenced by a package of young recycled oceanic crust with variable amounts of sediment. Combined with geophysical evidence, this demonstrates that recycling of ocean crust and marine sediments through the upper mantle from the MTZ can occur on relatively short time scales ($<$ 250 Myr), much faster than those associated with the plate deep subduction and mantle plume upwelling (possibly $>$ 1 Gyr). This new evidence shows that the production of mantle reservoirs enriched by the storage of past subducted slabs in the mantle transition zone is an important mechanism in the generation of distinctive isotopic domains that were generally thought to be related to deep recycling.

4. Our results show that marginal basins are important sites for introducing enriched oceanic and continental lithospheric material, i.e., chemical heterogeneity, into the upper mantle and transition zone. Subduction-induced upwelling from the mantle transition zone and nearby areas can explain the late Cenozoic volcanism observed in SE Asia.

CRediT authorship contribution statement

S.P.Q. collected the samples, performed much of the analytical work, and wrote the manuscript. H.Y.Z. collected the samples, conceived the project idea and revised the manuscript. V.S., A.J.M.-W., A.R.L.-N., K.H. and E.F.R.-K. contribute significant additions and edits to the manuscript. Melt inclusion and feldspars in situ Sr-Pb analyses, and melt inclusion trace element analyses were performed by engineer L.Z. J.W. drafted geophysical tomography figure and revised the manuscript. All authors participated in discussion and/or interpretation of results and gave valuable feedback on the manuscript.

Declaration of competing interest

The authors declare that they have no known competing financial interests or personal relationships that could have appeared to influence the work reported in this paper.

Acknowledgements

We are grateful for the very constructive reviews by two anonymous reviewers, and for the very useful suggestion by the editor Rosemary Hickey-Vargas, that all helped greatly to clarify several points in our manuscript. We are very grateful to Jenna V. Adams, Zhongyuan Ren, Yigang Xu, and Matthew G. Jackson for helpful discussions. We thank Anthony A.P. Koppers, Daniel P. Miggins, Lingmin Zhang and Hao Cheng for assistance in the sample analysis. This study was supported by the National Natural Science Foundation (NSF) of China (41902044 and 91428207) and the research grant of State Key Laboratory of Marine Geology (MGZ202201). Jonny Wu was supported by United States NSF grant EAR-1848327. Alex McCoy-West was supported by Australian Research Council grant DE210101395.

Appendix A. Supplementary material

Supplementary material related to this article can be found online at https://doi.org/10.1016/j.epsl.2022.117679.

References

Brandl, P.A., Beier, C., Regelous, M., Abouchami, W., Haase, K.M., Garbe-Schönberg, D., Galer, S.J.G., 2012. Volcanism on the flanks of the East Pacific Rise: quantitative constraints on mantle heterogeneity and melting processes. Chem. Geol. 289 (299), 41–56.

Briais, A., Patriat, P., Tapponnier, P., 1993. Updated interpretation of magnetic anomalies and seafloor spreading stages in South China Sea: implications for the Tertiary tectonics of Southeast Asia. J. Geophys. Res. 98, 6299–6328.

Castillo, P.R., Clague, D.A., Davis, A.S., Lonsdale, P.F., 2010. Petrogenesis of Davidson Seamount lavas and its implications for fossil spreading center and intraplate magmatism in the eastern Pacific. Geochem. Geophys. Geosyst. 11.

Chase, C.G., 1981. Oceanic island Pb: two-stage histories and mantle evolution. Earth Planet. Sci. Lett. 52, 277–284.

Chung, S.-L., Chu, M.-F., Zhang, Y., Xie, Y., Lo, C.-H., Lee, T.-Y., Lan, C.-Y., Li, X., Zhang, Q., Wang, Y., 2005. Tibetan tectonic evolution inferred from spatial and temporal variations in post-collisional magmatism. Earth-Sci. Rev. 68, 173–196.

Faccenna, C., Becker, T.W., Lallemand, S., Lagabrielle, Y., Funiciello, F., Piromallo, Claudia, 2010. Subduction-triggered magmatic pulses: a new class of plumes? Earth Planet. Sci. Lett. 299, 54–68.

Gale, A., Dalton, C.A., Langmuir, C.H., Su, Y.J., Schilling, J.G., 2013. The mean composition of ocean ridge basalts. Geochem. Geophys. Geosyst. 14, 489–518.

Haase, K.M., Regelous, M., Duncan, R.A., Brandl, P.A., Stroncik, N., Grevemeyer, I., 2011. Insights into mantle composition and mantle melting beneath mid-ocean ridges from post-spreading volcanism on the fossil Galapagos Rise. Geochem. Geophys. Geosyst. 12, Q0AC11.

Hanan, B.B., Graham, D.W., 1996. Lead and helium isotope evidence from oceanic basalts for a common deep source of mantle plumes. Science 272, 991–995.

Hanyu, T., Shimizu, K., Ushikubo, T., Kimura, J.-I., Chang, Q., Hamada, M., Ito, M., Iwamori, H., Ishikawa, T., 2019. Tiny droplets of ocean island basalts unveil Earth's deep chlorine cycle. Nat. Commun. 10, 60.

Hauff, F., Hoernle, K., Schmidt, A., 2003. Sr-Nd-Pb composition of Mesozoic Pacific oceanic crust (Site 1149 and 801, ODP Leg 185): implications for alteration of ocean crust and the input into the Izu-Bonin-Mariana subduction system. Geochem. Geophys. Geosyst. 4.

Hickey-Vargas, R., 1992. A refractory HIMU component in the sources of island arc magma. Nature 360, 57–59.

Hoang, N., Flower, M., 1998. Petrogenesis of Cenozoic basalts from Vietnam: implication for origins of a 'Diffuse Igneous Province'. J. Petrol. 39, 369–395.

Hoernle, K., Hauff, F., Werner, R., van den Bogaard, P., Gibbons, A.D., Conrad, S., Müller, R.D., 2011. Origin of Indian Ocean Seamount Province by shallow recycling of continental lithosphere. Nat. Geosci. 4, 883.

Höfig, T.W., Geldmacher, J., Hoernle, K., Hauff, F., Duggen, S., Garbe-Schönberg, D., 2014. From the lavas to the gabbros: 1.25 km of geochemical characterization of upper oceanic crust at ODP/IODP Site 1256, eastern equatorial Pacific. Lithos 210–211, 289–312.

Hofmann, A.W., 1997. Mantle geochemistry: the message from oceanic volcanism. Nature 385, 219–229.

Jackson, M.G., Hart, S.R., 2006. Strontium isotopes in melt inclusions from Samoan basalts: implications for heterogeneity in the Samoan plume. Earth Planet. Sci. Lett. 245, 260–277.

Kamenetsky, V.S., Crawford, A.J., Eggins, S., Muhe, R., 1997. Phenocryst and melt inclusion chemistry of near-axis seamounts, Valu Fa Ridge, Lau Basin: insight into mantle wedge melting and the addition of subduction components. Earth Planet. Sci. Lett. 151, 205–223.

Kent, A.J.R., 2008. Melt inclusions in basaltic and related volcanic rocks. Rev. Mineral. Geochem. 69, 273–331.

Li, C., van der Hilst, R.D., 2010. Structure of the upper mantle and transition zone beneath Southeast Asia from traveltime tomography. J. Geophys. Res. 115, B07308.

Li, C.-F., Xu, X., Lin, J., Sun, Z., Zhu, J., Yao, Y., Zhao, X., Liu, Q., Kulhanek, D.K., Wang, J., Song, T., Zhao, J., Qiu, N., Guan, Y., Zhou, Z., Williams, T., Bao, R., Briais, A., Brown, E.A., Chen, Y., Clift, P.D., Colwell, F.S., Dadd, K.A., Ding, W., Almeida, I.H., Huang, X.-L., Hyun, S., Jiang, T., Koppers, A.A.P., Li, Q., Liu, C., Liu, Z., Nagai, R.H., Peleo-Alampay, A., Su, X., Tejada, M.L.G., Trinh, H.S., Yeh, Y.-C., Zhang, C., Zhang, F., Zhang, G.-L., 2014. Ages and magnetic structures of the South China Sea constrained by deep tow magnetic surveys and IODP Expedition 349. Geochem. Geophys. Geosyst. 15, 4958–4983.

Li, Z.-X., Li, X.-H., 2007. Formation of the 1300-km-wide intracontinental orogen and postorogenic magmatic province in Mesozoic South China: a flat-slab subduction model. Geology 35, 179–182.

Lin, J., Xu, Y.G., Sun, Z., Zhou, Z.Y., 2019. Mantle upwelling beneath the South China Sea and links to surrounding subduction systems. Nat. Sci. Rev. 6 (5), 877–881.

Mather, B.R., Müller, R.D., Seton, M., Ruttor, S., Nebel, O., Mortimer, N., 2020. Intraplate volcanism triggered by bursts in slab flux. Sci. Adv. 6 (51), eabd0953.

Mazza, S.E., Gazel, E., Bizimis, M., Moucha, R., Béguelin, P., Johnson, E.A., McAleer, R.J., Sobolev, A.V., 2019. Sampling the volatile-rich transition zone beneath Bermuda. Nature 569, 398.

McCoy-West, A.J., Bennett, V.C., Amelin, Y., 2016. Rapid Cenozoic ingrowth of isotopic signatures simulating "HIMU" in ancient lithospheric mantle: distinguishing source from process. Geochim. Cosmochim. Acta 187, 79–101.

Mei, S.W., 2018. The Petrogenesis and Geodynamic Mechanism of Late Cenozoic Basalts in North Hainan Island. MSc thesis (in Chinese with English abstract). University of Chinese Academy of Science, Beijing.

Meibom, A., Anderson, D.L., 2004. The statistical upper mantle assemblage. Earth Planet. Sci. Lett. 217, 123–139.

Peate, D.W., Peate, I.U., Rowe, M.C., Thompson, J.M., Kerr, A.C., 2012. Petrogenesis of high-MgO lavas of the lower mull plateau group, Scotland: insights from melt inclusions. J. Petrol. 53, 1867–1886.

Qian, S., Gazel, E., Nichols, A.R.L., Cheng, H., Zhang, L., Salters, V.J., Li, J., Xia, X.P., Zhou, H.Y., 2021. The origin of late Cenozoic magmatism in the South China Sea and Southeast Asia. Geochem. Geophys. Geosyst. 22.

Qian, S.P., Ren, Z.Y., Richard, W., Zhang, L., Zhang, Y.H., Hong, L.B., Ding, X.L., Wu, Y.D., 2017. Petrogenesis of Early Cretaceous basaltic lavas from the North China Craton: implications for cratonic destruction. J. Geophys. Res. 122, 1900–1918.

Ramos, F., Tepley III, F., 2008. Inter- and intracrystalline isotopic disequilibria: techniques and applications. Rev. Mineral. Geochem. 69.

Rose-Koga, E., Koga, K., Moreira, M., Vlastélic, I., Jackson, M., Whitehouse, M.J., Shimizu, N., Habib, N., 2017. Geochemical systematics of Pb isotopes, fluorine, and sulfur in melt inclusions from São Miguel, Azores. Chem. Geol. 458.

Salters, V.J.M., Stracke, A., 2004. Composition of the depleted mantle. Geochem. Geophys. Geosyst. 5.

Sibuet, J.C., Yeh, Y.C., Lee, C.S., 2016. Geodynamics of the South China Sea. Tectonophysics 692, 98–119.

Sobolev, A.V., Hofmann, A.W., Jochum, K.P., Kuzmin, D.V., Stoll, B., 2011. A young source for the Hawaiian plume. Nature 476, 434–U483.

Stracke, A., Bizimis, M., Salters, V.J.M., 2003. Recycling of oceanic crust: quantitative constraints. Geochem. Geophys. Geosyst. 4, 8003.

Stracke, A., Hofmann, A.W., Hart, S.R., 2005. FOZO, HIMU, and the rest of the mantle zoo. Geochem. Geophys. Geosyst. 6.

Sun, S.-S., McDonough, W.F., 1989. Chemical and Isotopic Systematics of Oceanic Basalts: Implications for Mantle Composition and Processes. Special Publications, vol. 42. Geological Society, London, pp. 313–345.
Tao, K., Grand, S.P., Niu, F., 2018. Seismic structure of the upper mantle beneath eastern Asia from full waveform seismic tomography. Geochem. Geophys. Geosyst. 19, 2732–2763.
van der Hilst, R.D., Widiyantoro, S., Engdahl, E.R., 1997. Evidence for deep mantle circulation from global tomography. Nature 386, 578–584.
Wang, X.C., Li, Z.X., Li, X.H., Li, J., Xu, Y.G., Li, X.H., 2013. Identification of an ancient mantle reservoir and young recycled materials in the source region of a young mantle plume: implications for potential linkages between plume and plate tectonics. Earth Planet. Sci. Lett. 377, 248–259.
Wang, Y.J., Han, X.Q., Luo, Z.H., Qiu, Y.Z., Ding, W.W., Li, J.B., Gao, S.T., Chen, R.H., 2009. Late Miocene magmatism and evolution of Zhenbei-Huangyan Seamount in the South China Sea: evidence from petrochemistry and chronology. Acta Oceanol. Sin. 31, 93–102.
Workman, R.K., Hart, S.R., 2005. Major and trace element composition of the depleted MORB mantle (DMM). Earth Planet. Sci. Lett. 231, 53–72.
Wu, H.H., Tsai, Y.B., Lee, T.Y., Lo, C.H., Hsieh, C.H., Toan, D.V., 2004. 3-D shear wave velocity structure of the crust and upper mantle in South China Sea and its surrounding regions by surface wave dispersion analysis. Mar. Geophys. Res. 25, 5–27.
Yan, Q., Shi, X., Metcalfe, I., Liu, S., Xu, T., Kornkanitnan, N., Sirichaiseth, T., Yuang, L., Zhang, Y., Zhang, H., 2018. Hainan mantle plume produced late Cenozoic basaltic rocks in Thailand, Southeast Asia. Sci. Rep. 8, 2640.
Zhang, G.-L., Luo, Q., Zhao, J., Jackson, M.G., Guo, L.-S., Zhong, L.-F., 2018. Geochemical nature of sub-ridge mantle and opening dynamics of the South China Sea. Earth Planet. Sci. Lett. 489, 145–155.
Zhao, D.P., Yu, S., Ohtani, E., 2011. East Asia: seismotectonics, magmatism and mantle dynamics. J. Asian Earth Sci. 40, 689–709.
Zindler, A., Hart, S., 1986. Chemical geodynamics. Annu. Rev. Earth Planet. Sci. 14, 493–571.
Zou, H.B., Fan, Q.C., 2010. U-Th isotopes in Hainan basalts: implications for subasthenospheric origin of EM2 mantle endmember and the dynamics of melting beneath Hainan Island. Lithos 116, 145–152.